COMPREHENSIVE MODELLING OF FLEXIBLE ROTOR BLADE AND ITS POWER TRAIN

J. Kumar, A. Lass, F.-H. Wurm,
University of Rostock, Faculty of Mechanical Engineering and Marine Technology, Institute of Turbomachinery
Albert-Einstein-Str. 2, 18059 Rostock, DE

Abstract

A mixer propeller is used in sewage application to keep particles in water suspended and therefor provides kinetic energy to fluid for plug flow. This system has several mechanical components like blades, hub, shaft, gearbox, bearings and induction motor. Its power-train is a complex, nonlinear multi-energy domain system. Specialized tools and commercial software have been developed in last few decades to model different physical domains individually. To overcome modelling problem, bond graph (BG) methodology is used to model the entire power-train where every element is attached to its neighbor using power bonds considering physical causality. Formerly two-way fluid-structure interaction (FSI) is performed for the propeller blade using Ansys-CFX and Ansys-APDL solver code. k-ω SST turbulence model is used for computational fluid dynamic simulation (CFD) to calculate torque and thrust on the blades. Damping coefficient and averaged flow-induced forces are calculated based on transient result of two-way FSI. Further averaged flow-induced forces including damping coefficient are communicated to the blade nodes in BG model. By this uni-directional FSI (weak coupling) is setup for rotor dynamic analysis of mixer power-train using BG. Hydrodynamic mass of water on structural system is not yet considered. The BG methodology combined with CFD can be used to develop a reliable, robust and agile technique for multi-energy domains systems including FSI. Transient analysis and frequency spectrum is plotted for blade and whole rotating system. Effect of eccentricity and CFD loading is analyzed thoroughly. The strong coupling of CFD and BG including fluid-induced forces due to the dynamics of involved system components like motor, gearbox and hub is kept as future work for research.

1. INTRODUCTION

Mixers are used for homogenization of sewage and to prevent sedimentation in tanks, channels or oxidation ditches. They are designed to generate fluid flow in the tank behind the propelling blade. The propeller delivers kinetic energy to the fluid and keeps particles in suspension through frictional forces [1]. The power-train of such rotating system consists of an electric motor, bearings, gearbox, spinning shaft, hub and blades, as presented in Fig. 1.

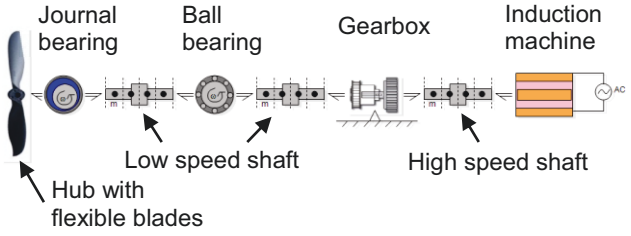

Figure 1. Representative assembly of mixer power train system

During rotation, the propeller experiences thrust and torque which causes blade deformations. Accurate prediction of thrust and torque using CFD techniques is extremely important for FSI simulation. Tian et al. [2] performed numerical simulations of submersible mixers with two blades using FLUENT with a tetrahedral mesh. Kumar et al. [3] studied the effects of mixer blade geometry and deformation on jet flow shape and sedimentation. The importance of thrust and torque is well understood, but numerical simulation for studying jet flow behavior with appropriate turbulence model to calculate correct thrust and torque values is still an open issue. Furthermore it is hard to find a suitable platform or technique to model and simulate rotor dynamic behavior of a complex multi-energy domain system including non-linear effects of various hydrodynamic and structural domains.

The bond graph methodology is a suitable approach to create models of a complex dynamic system considering the interaction of several energy domains. This method was invented by Paynter [4] and further elaborated from a graphical model to a methodology by the Karnopp, Margolis and Rosenberg [5]. The application of BG and the modelling of diverse engineering systems with various physical domains can be found in [6-10]. The method generally provides more physical insights to visualize the rotor dynamics phenomena from energy flow and visual prospective due to the energy based nature of its basic modelling elements (inertial, complaint and resistive elements). Several software that support BG modelling and simulation have been developed like 20sim, symbols sonata, CAMP-G and further more. Using BG for rotor dynamic analysis was studied by [11] with limitation to simple models and structural domain only. Sanchez and Medina [12] created a more detailed BG model for a wind turbine and analyzed its power output behavior including structural dynamics (no rotor dynamics). The rotor dynamics analysis of a mixer propeller inside water is complicated because of high flow and vibration induced forces acting on the system. Van Esch et al. [13] quantified the hydrodynamic forces due to torsional and axial vibration using CFD to calculate hydrodynamic propeller coefficient for added mass and quasi-steady fluid-induced damping. Still comprehensive modelling of a complete power train of mixer propeller power train including induction motor, gearbox, shaft, hub and blade with CFD loads is relatively scarce. Multi-energy domain modelling combined with rotor dynamics including CFD and eccentric load is an open issue which will be comprehensively analyzed in this paper. BG methodology is selected to model the power train of a mixer system because this method provides platform to model power exchange, energy dissipation and storage in a dynamic system of any physical domain with a unified graphical language. A parametric and generic model of the propeller system can be used for any size of power-train to

predict life and real time behavior at various boundary conditions. Therefor an integrated generic BG model can reduce pre-processing and prototype creation time during the development of new propeller or turbine systems.

The main objective of the paper is to perform a comprehensive simulation of a multi-energy domain for a mixer power-train system using CFD, Ansys-APDL and BG methodology. The first goal of the current research is to understand the flow behavior, the thrust and torque behind the mixer with variation in inlet velocity using CFD. Then bi-directional FSI of propeller blade is performed to calculate fluid damping coefficient and fluid induced forces. The next aim is to model a mixer power-train system using the BG methodology keeping their physics in foreground. The final objective of this paper is to analyze blade deformations, shaft vibration amplitudes and the dynamic behavior of the rotating components for industrial purposes using CFD forces and damping coefficient of the fluid.

2. CFD MODELLING

The state of the art for analyzing rotating propellers can be seen in Fig. 2 that defines the stator and rotor domains. Propellers push forward the fluids and generate a swirl jet flow at the same time. Quality of the mesh plays an important factor for the convergences of simulations and accuracy of results. Hence the high quality hex-mesh was created (Fig. 3), with minimum angle greater than 27^0 using the blocking concept in ICEM meshing software. Normalized wall distance, y^+, was maintained equal to one on the blade surface to capture the laminar sub layer and velocity distribution correctly. Boundary conditions were set such that, at the inlet, velocity was defined normal to the surface and zero pressure was assigned at the outlet. The rotating speed of blade and rotor domain was set at 46 RPM. The general grid interface mesh connection was used for the rotor-stator interface. In this current work, *k-ω* SST turbulence model was used for closure. The transient terms were calculated with a second order backward Euler scheme and integration of the advection terms were approximated by a high resolution scheme. Transient rotor-stator coupling was used to account for transient interactions of the rotating impeller domain with the stationary domains. The curvature correction term and Kato-Launder production limiter for turbulence model was applied. 10^{-4} *MAX* numerical convergence limit was reached for transient simulation.

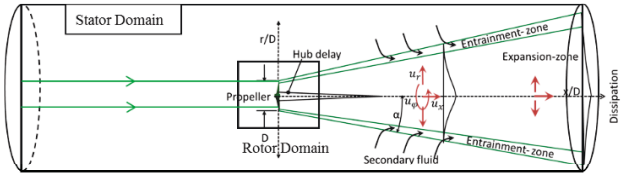

Figure 2. Schematic view of stator and rotor domain and theoretical flow behaviour

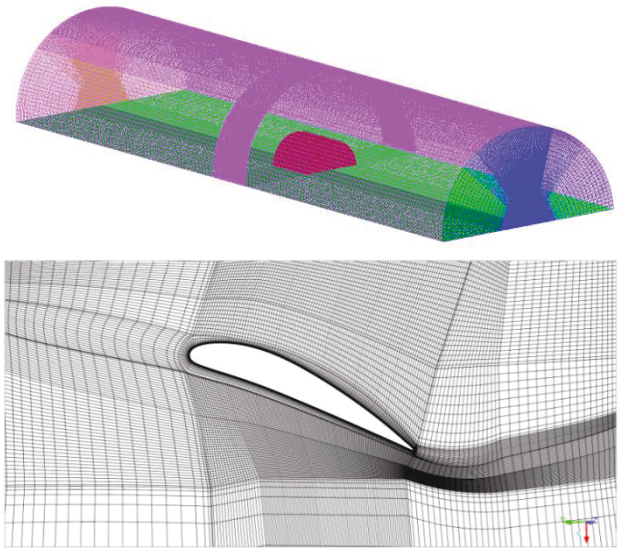

Figure 3. Hex grid of the fluid domain (top) and grid around the blade (bottom)

2.1. CFD Simulation Results

Analysis explains that, the thrust and torque increase with decrease in inlet velocity and thereafter become constant as shown in Fig. 4. At constant power supply, thrust increases with decrease of inlet velocity. Normally, experiments are performed in a pond only in case of still water so that inlet velocity can be assumed as zero. Calculated thrust and torque data based on experiment is plotted in Fig. 4. Experiments are not performed for other velocities due to an unsteady inflow condition for the propellers in a pond. As power law of propeller suggest [3] that maximum thrust and torque would be at zero inlet velocity. Numerical results are also showing maximum thrust and torque at zero inlet velocity. Values are matching to experimental value at zero m/s inlet speed. This shows correctness of the numerical setup and accuracy in numerical calculation.

For 0.2 m/s axial inlet speed the maximum axial velocity and circumferential velocity are displayed in Fig. 5 which indicates that both the velocities decreases with the distance from the mixer and later becomes constant. Also, Fig. 5 illustrates the flow pattern at different distances from the mixer. Axial velocity at centre of plane is smaller than maximum axial velocity on same plane because of hub vortex. Based on comparison of experimental results and theoretical understanding of the flow behind the mixer to the numerical simulation results, the used CFD model for fluid domain is considered to work correctly. Moreover this numerical model is suitable to be used for bi-directional FSI.

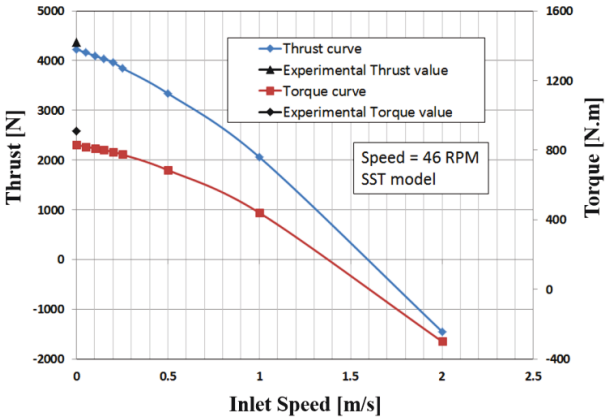

Figure 4. Thrust and torque curve vs. inlet speed

2.2. Bi-directional Fluid-Structure-Interaction

The bi-directional iterative implicit modelling approach was used for simulation using a mesh smoothing method. The fluid and structural solvers were solved separately, and the data were transferred using a mapping technique. A transient bi-directional iterative implicit FSI has three levels of iteration: 'time loop', 'coupling loop' and 'field loop'. The field loop is the most inner loop which was used to converge the flow field within a solver. It stops when the flow field variables reached their convergence target. At the coupling loop, load and displacement were transferred using a mapping method between the fluid and structural solver. It stops when both the force and the displacement converged. Time loop was advancement in real-time transient simulation. The simulation was performed for 0.5 [s]with a 0.001 [s] increment time step, 5 coupling iterations per loop and 200 field convergence iterations for each inlet speed. Numerically calculated total deformation is plotted in Fig. 6 including a damping function curve. This damping curve includes both structural and fluid damping. After filtering a structural damping 0.2 [Ns/m] damping coefficient of water was estimated.

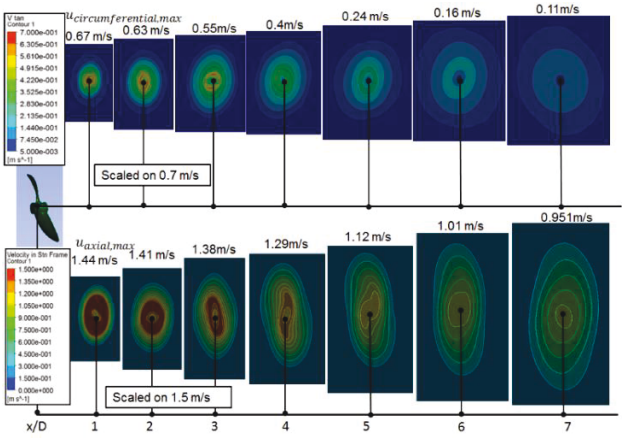

Figure 5. Axial and circumferential velocity profile at different axial positions

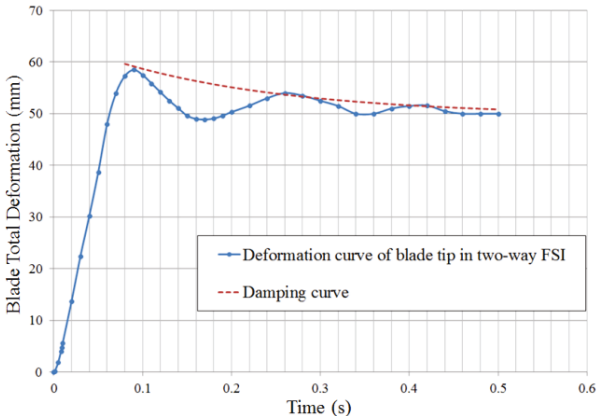

Figure 6. Total deformation and damping curve of blade in two-way FSI

To map the CFD load entire blade was divided into seven sections as shown in Fig. 7 then forces and moments in all direction for each section were calculated as provided in Tab.1. For BG model of the blade, mass and stiffness (based on second moment of area) for each sections were calculated.

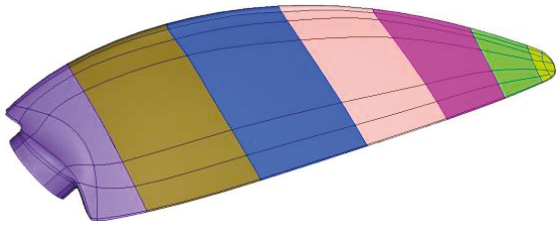

Figure 7. Seven sections defined of the blade used for mapping of data from CFD to BG

Section	1	2	3	4	5	6	7
Fx [N]	-35	-218	-462	-539	-493	-232	-50
Fy [N]	-48	-103	-149	-136	-86	-15	-5
Fz [N]	-32	0.03	1	-11	1.6	18	-1.5
Mx [Nm]	1.7	-3.6	-6.2	-6.1	-4.4	-1.2	-0.1
My [Nm]	-2.6	2.4	7.1	8.3	7.7	3.7	0.4
Mz [Nm]	1.9	5.1	6.5	4.0	0.8	1.0	0.1

Table 1. Fluid forces and moments for seven sections calculated from CFD and mapped on blade nodes in BG

3. BOND GRAPH MODELLING

The basic variables in bond graph are effort (*e*), flow (*f*), time integral of effort (*p*) and time integral of flow (*Q*). Effort & flow for electrical and structural system are voltage & current and force & velocity respectively. Power bonds join at 1 junctions summing efforts to zero with equal flows or at 0 junctions summing flows to zero with equal efforts. These junctions are not physical elements. The basic single port bond graph elements are source of effort, source of flow, inertial compliant and resistive elements represented as *SE, SF, I, C* and *R* respectively. Basic 2-port elements are transformer and gyrators used for power transformation represented as TF and GY in BD methodology. Equation (1) shows a generalised system equation used in BG, where

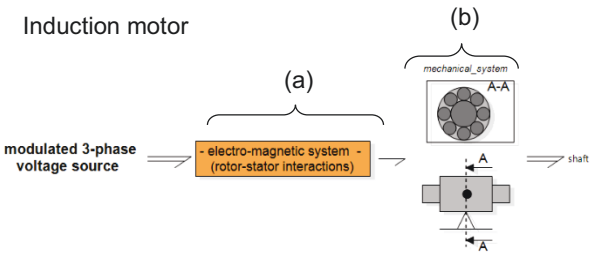

Electro-magnetic subsystem (a):

- Stator, rotor electrics and magnetic coupling

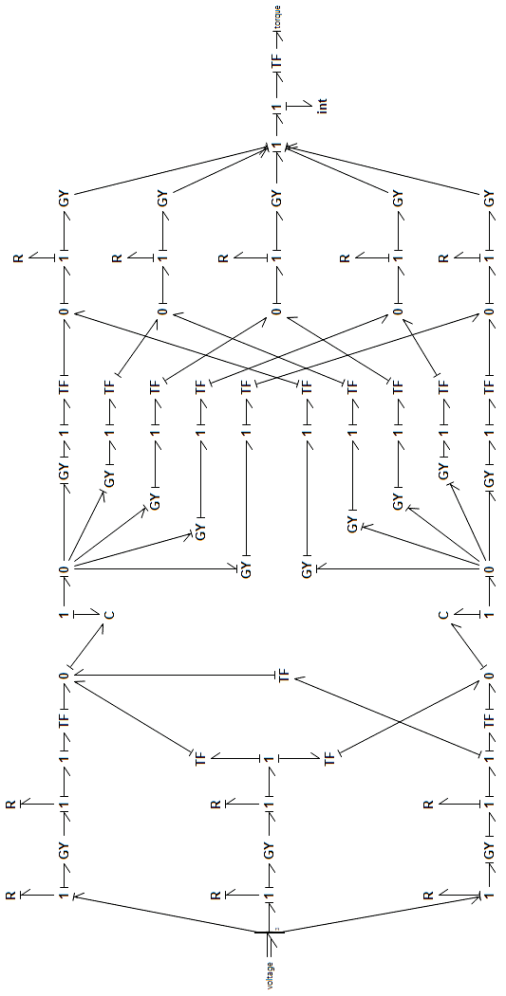

Mechanical subsystem:

- rigid body motor shaft (b)

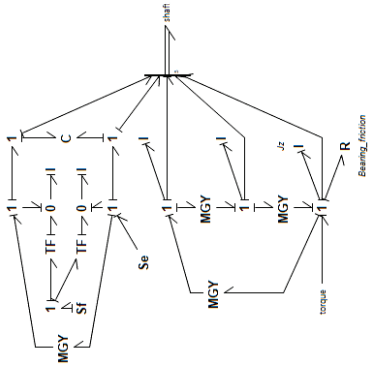

Figure 8. Bond graph model of squirrel cage induction motor

{X} is the state vector, *{U}* is the input vector, *{A}* is the system matrix and *{B}* is the input matrix. This methodology derives system equations in matrix form for all basic variables based on a model and solves the generated differential equations. From the next paragraph onward the BG model for each component of power-train system is discussed.

$$\frac{\partial}{\partial t}\{X\} = [A]\{X\} + [B]\{U\} \tag{1}$$

3.1. Components of power train

The **Induction motor** BG model was composed into two major sub-model: a rotating rotor and a stationary stator. The induction motor was modelled and designed with a sinusoidal distribution of stator winding voltage throughout air gap. The magnetic losses, air gap losses and core losses were also considered [14].The different transformations from one domain to another domain have been explained by [14-16]. A detailed model of the induction motor is presented in Fig. 8.

The **spinning shaft** is the rotating component of the system. The shear forces and moments acting on the shaft element were modelled. Inertia and stiffness in stationary frame, as well as internal damping in rotating frame of the shaft relate generalized Newtonian forces to generalized acceleration, displacements and velocity at the end of the element respectively [10]. The shaft model for the mixer power-train system was divided into a number of small elements and each element was modelled as the Rayleigh beam as demonstrated in Fig. 9(a) [10]. Each shaft element contains two sub-model, mass element and spring element as presented in Fig. 9 (b) and (c). Every element of the spinning shaft has five degrees of freedom which are translational in Y and Z direction and rotation around all axes. The gyroscopic effect was also considered.

The **gear box** consists of toothed wheels used for the transmission of power in mechanical systems. When two gears are meshed, a definite gear ratio is obtained. The gear ratio is the ratio between the angular velocity of the driving gear and the angular velocity of the driven gear. A transfer function element was used to represent the gear ratio of the system.

Ball bearings assure the smooth operation of the machines by providing support to the rotary parts and by reducing the friction. This module was modelled with linear contact stiffness as defined in Eq. (2). However, the bearing reaction force was modelled non-linear as described in Eq. (3), where *E, ρ, δ*, ν* and *δ* are modulus of elasticity, curvature, non-dimensional deflection factor, Poisson's ratio and generalised deformation respectively. Rayleigh damping was considered in the term of geometrical description of bearing. Its formulation was based on Hertzian theory [17]. The input of the model was vectorised with two translational and three rotational velocities in fixed frame and the output was also vectorised with the same attributes.

$$K = \frac{2E\sqrt{2}}{3\delta^{*3/2}(\rho)^{1/2}(1-\nu^2)} \tag{2}$$

$$F = K\delta^{3/2} \tag{3}$$

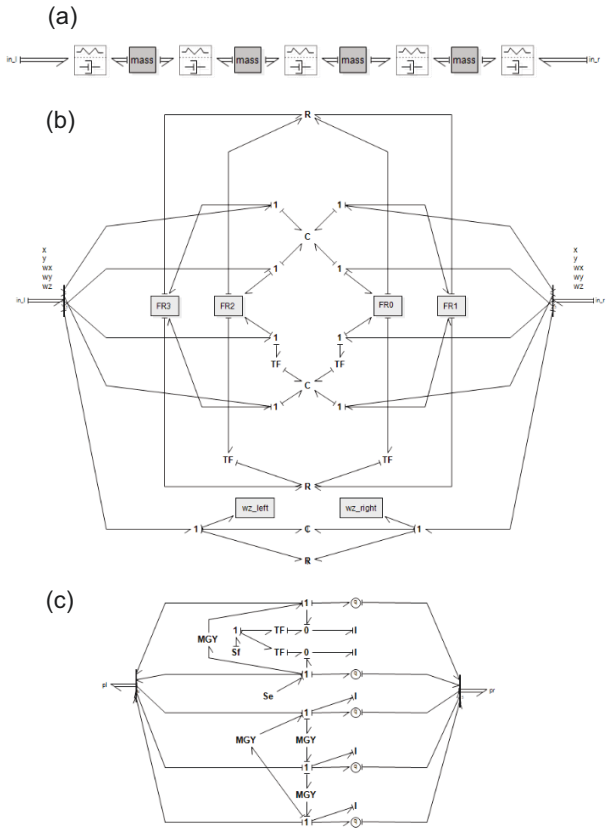

Figure 9. Bond graph model of spinning shaft assembly (a) using springer-damper (b) and mass (c) element

The **Spinning hub** was modelled as annular disks. The model incorporates the eccentricity of hub centre mass (Fig. 10). Its angular orientation was recorded by the flow-activated element. The gyroscopic coupling was also included in the module along with eccentricity. Eccentricity of the spinning hub was modelled to transformer elements, where Ω is excitation frequency of the shaft, $\emptyset$ is the initial angle between shaft midpoint and unbalanced mass measured from the vertical axis and ε is the eccentricity.

$$\mu_1 = -\varepsilon \sin(\Omega t + \phi), \mu_2 = \varepsilon \cos(\Omega t + \phi)$$

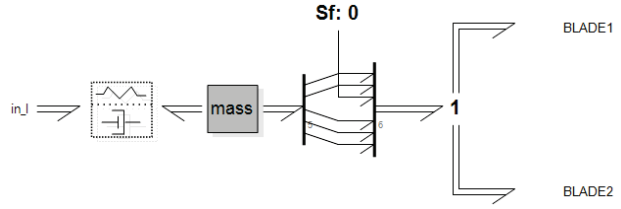

Figure 10. Bond graph model for hub composed by spring-damper and mass element (see Figure 9) as well as axial fixation and 1-junction to connected blades.

The **propeller blade** used for this system was modelled as a three-dimensional isotropic cantilevered Rayleigh beam with varying cross-sectional parameters. The blade system was modelled based on FEM formulation to represent the exactness of the system within bond graph. The Rayleigh beam element captures translational as well as rotational inertias in all directions (six degree of freedom). The blade was divided into seven flexible beam elements as demonstrated in Fig. 12. Averaged fluid forces were mapped from CFD simulation to blade nodes.

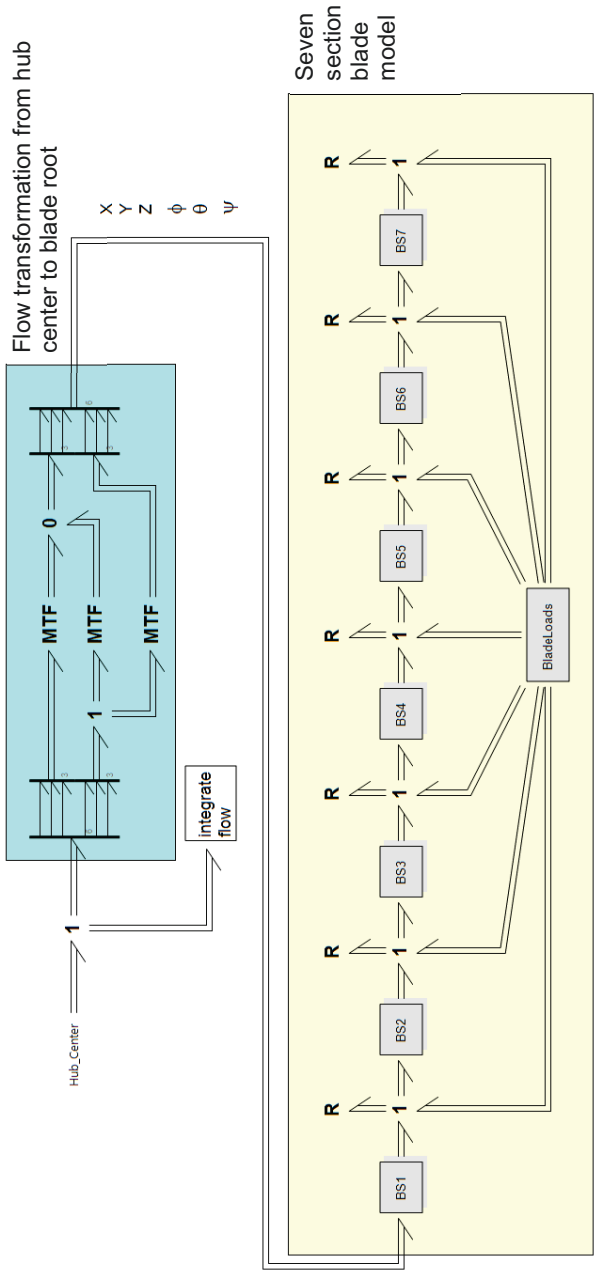

Figure 11. Bond graph model of seven section blade with transformation between hub center and blade root

The **journal bearing** produces smooth motion between solid surfaces in relative motion and generates a load support for mechanical components. The journal bearing was used in the system just before the rotating hub as displayed in Fig. 11. The non-linear hydrodynamic forces [18] in the *r* direction and the θ direction for a finite full film bearing are defined in Eq. 5 and 6 where ε, θ, ϕ, R, ω, C and L are eccentricity ratio, reference angle, attitude angle, radius, rotational speed, clearance and length of bearing respectively.

$$F_r = 2\int_{-L/2}^{L/2}\int_{0}^{2\pi} RP(\theta,z)\cos\theta\, d\theta\, dz = \frac{24\pi R^3 \dot{\varepsilon}}{C^2\left(1-\varepsilon^2\right)^{3/2}}\left[L - \frac{2R\tanh K_2 L/2R}{K_2}\right] \quad (5)$$

$$F_\theta = 2\int_{-L/2}^{L/2}\int_{0}^{2\pi} RP(\theta,z)\sin\theta\, d\theta\, dz = \frac{24\pi R^3 \varepsilon(\omega - 2\dot{\phi})}{C^2\left(2+\varepsilon^2\right)\left(1-\varepsilon^2\right)^{1/2}}\left[L - \frac{2R\tanh Q_2 L/2R}{Q_2}\right] \quad (6)$$

$$K_2 = \frac{(2\varepsilon)^{1/2}}{\left(1-\varepsilon^2\right)^{1/2}} \quad (7)$$

$$Q_2 = \left[\frac{4+2\varepsilon^2+4\sqrt{1-\varepsilon^2}+2\varepsilon^2\sqrt{1-\varepsilon^2}}{4-4\varepsilon^2+4\sqrt{1-\varepsilon^2}-\varepsilon^2\sqrt{1-\varepsilon^2}}\right]^{1/2} \quad (8)$$

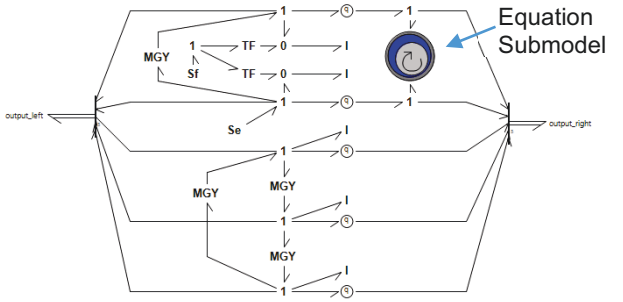

Figure 12. Bond graph model of journal bearing mass with equation submodel for hydrodynamic load estimation.

3.2. Impact test

The integrated bond graph model for a power-train has been presented in Fig. 1. Initially, an impact test was performed numerically for the BG model. Natural frequencies were obtained by imparting impulsive forces in both translational and circumferential directions at the respective mass elements of the hub. Therefore, the angular velocity and the damping coefficients were set to zero. FFT was applied on the displacement signals to obtain the natural frequencies. Fig. 13 shows the frequency responses to reveal the critical speeds. The first lateral frequency is determined at 18 Hz. Other frequencies were observed at 42 Hz and 54 Hz, with their harmonics following in the spectrum.

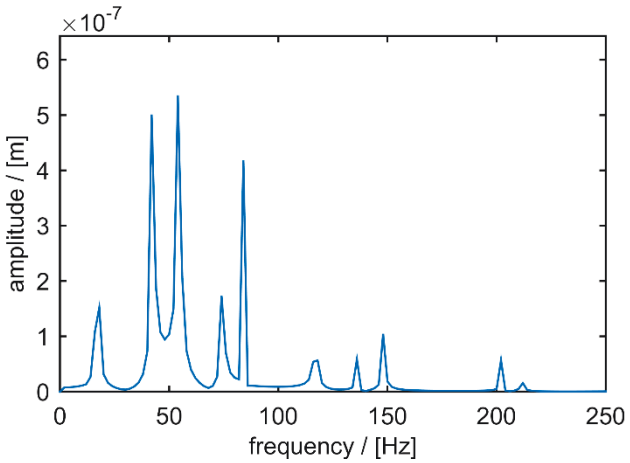

Figure 13. Frequency spectrum of X-displacement due to impact on hub

Figure 14 shows the transient behavior of the system with damping when an impulsive force is imparted in the translational direction of hub. Initially the system is having high displacements that were gradually damped. The plots in the figure show the response of all mass element modules of the power train. The hub was a free end body having maximum mass, hence vibrating at highest amplitudes.

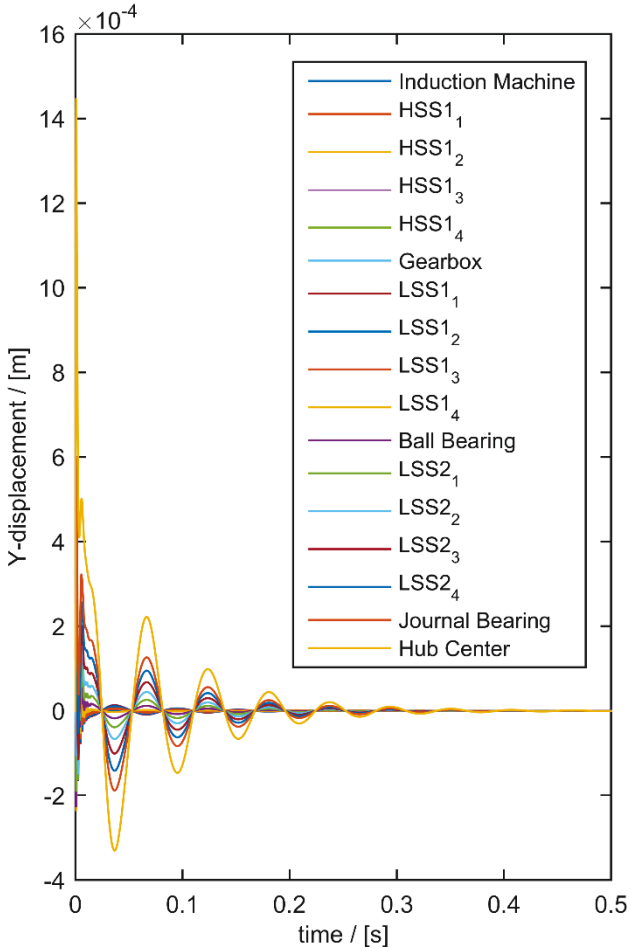

Figure 14. Time-dependent displacement of power train components after impulsive force application on hub in Y-direction

3.3. Transient analysis

Initializing input voltage and fluid forces – Figure 15 shows the behavior of the rotor velocity (left vertical axis) which reaches a steady state after t=1 [s]. Ideally the slip between rotor and stator is zero at steady state because the rotating frequency has the same frequency grid voltage (see Fig. 15 right vertical axis). Due to induction machine physics slip is observed under loading conditions. While start-up loads are related to mechanical losses only. Hence slip converges to a very small value of $S = 0.0027$. A gear ratio equal to 62.2 is used to reduce the induction machine rotor speed of 3000 [rev/min] to connected low speed power train components like hub and blades. Fluid forces are assumed to linearly vary with rotational speed of hub reaching their original values at 46 [rev/min] as defined in FSI-Simulation. As a result the blade is loaded while initialization and blade deflection can be

computed integrating the global velocity components of each blade section (see Figure 16)

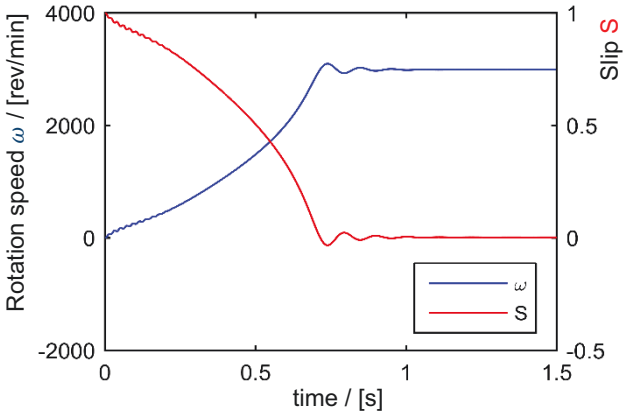

Figure 15. Rotational speed of induction machine rotor and slip between rotor and stator domain while start-up

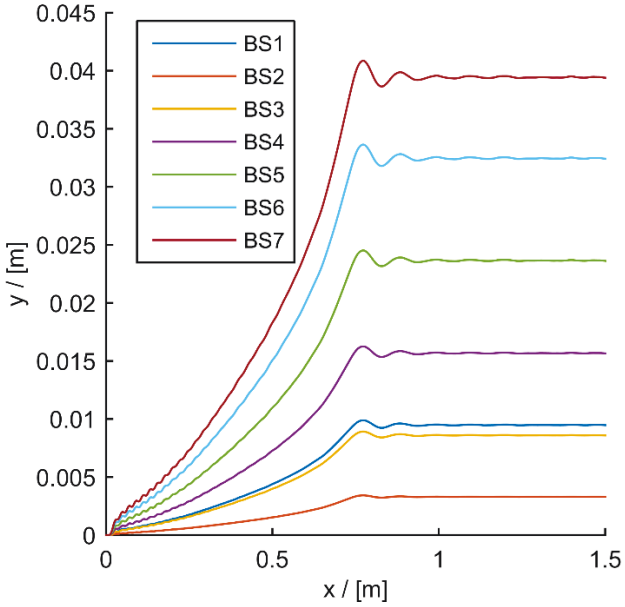

Figure 16. Total Displacement of blade section while initialization of rotation and increasing fluid-forces

Bond Graph Methodology allows a detailed power analysis of all used components. By modelling the induction machine the power input and output as well as losses in stator/rotor windings and magnetic flux are modelled using resistive elements. In Figure 16 the total power of induction machine stator and rotor is plotted against time at the startup procedure. It can be observed the stator power, which correlates to electric power input is always above rotor power, which can be read as mechanical input power neglecting all mechanical losses. The converged results of power analysis under operating conditions can be found in table 2. Using the transient simulation it is possible to estimate the efficiency of a system and optimize its general properties by a parametric variation of selected characteristics.

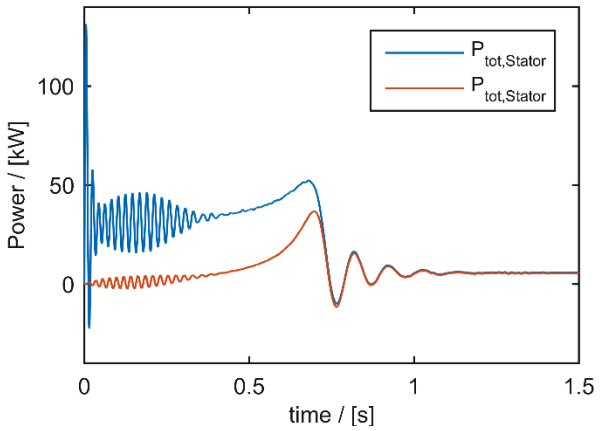

Figure 17. Total stator and rotor power of induction machine

Table 2. Power analysis of induction machine

Stator electric power input:	$P_{S,I}$	5.848 kW
Stator winding losses:	$P_{S,L}$	0.313 kW
Rotor winding losses:	$P_{R,L}$	0.0165 kW
Magnetic flux losses:	$P_{M,L}$	0.00062 kW
Rotor mechanical output:	$P_{R,O}$	5.518 kW
Efficiency:	$\eta = \frac{P_{R,O}}{P_{S,I}}$	≈94%

Influence of eccentricity and gravity – Using the results from previous investigations as initial conditions for further analysis a strong eccentricity of 8.25x10^{-2} [m] is added to the hub mass. The related centrifugal forces then lead to a continuous excitation of the shaft. This transient simulation is taken for 10 [s]. After that, the gravitational acceleration of 9.81 [m/s²] is applied to all mass elements of the system to account for gravity effects. The main idea behind of this process is to investigate their impact to the rotor dynamic behavior of the mixer power-train.

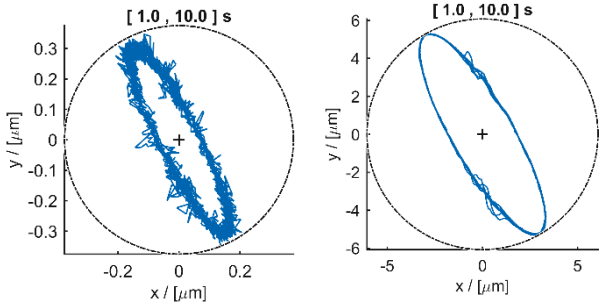

Figure 18. Orbital path of gearbox (left) and hub (right) between considering eccentricity

In Fig. 18 the orbital behavior of representative modules of the system from 1 [s] to 10 [s] is plotted. The time range is limited, because large amplitudes occur within the first second when eccentricity is suddenly introduced and then is changing into orbital behavior. The factors that influence the system to undergo the orbital movement are reverse forces, angular velocity and the gyroscopic effect.

By adding gravitational acceleration in negative y -direction of the system and neglecting counteracting buoyancy forces on the propeller the power train is bend within its mounting. Due to highest mass of hub with

attached propeller blades it observes highest negative displacement, whereas the gearbox is lifted upwards as a result of the intermediate bearing support. In consequence of cross-coupled journal bearing stiffness the hub is moving towards positive x-direction and the gearbox contrary (see Figure 19).

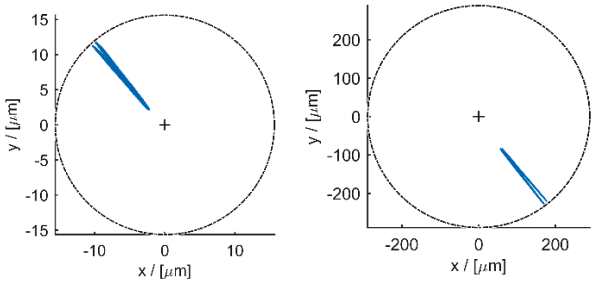

Figure 19. Orbital path of gearbox (left) and hub (right) considering eccentricity and gravity

Dealing with transient simulations like rotor dynamics a FFT-analysis can be conducted to extract whirl frequency of a selected component. Utilizing the y-component from orbital path plot subtracting its time averaged displacement value a vibration amplitude vs. time signal of hub mass center is derived.

Analyzing the case with eccentricity the first and major whirl mode to be found is at 0.78 [Hz], which directly correlates to the angular speed of 46 [rev/min] at hub center. The corresponding signal and frequency spectrum is shown in Figure 20.

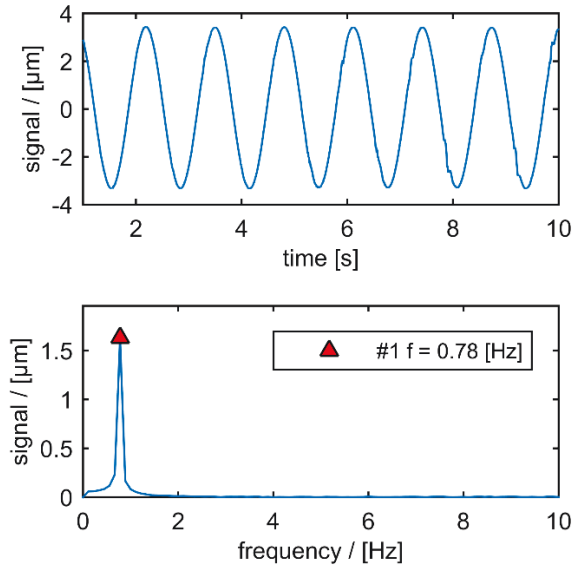

Figure 20. Vibration signal of y-displacement (top) and derived result of FFT-analysis with detected whirl modes (bottom). Case: effect of eccentricity.

In Figure 21 the effect of eccentricity and gravity is analysed as discussed previously. The first whirl mode identified is also identical to 0.78 [Hz], but the major whirl amplitude is found with a frequency 1.56 [Hz]. The excitation of a rotating system with a frequency which is twice of its operation speed is referred to as super synchronous whirl. It is a result of the strong misalignment of the shaft due to gravitational load. The elliptical orbit shape which can be found with eccentricity only is altered to a loop line when gravity is considered, with the aforementioned effect on the whirling modes.

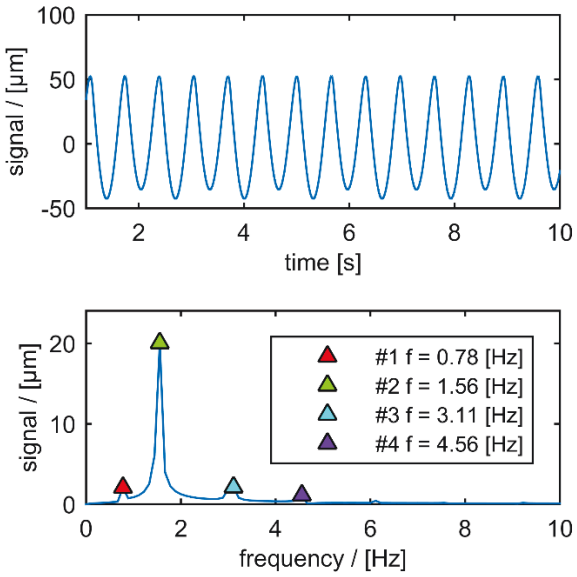

Figure 21. Vibration signal of y-displacement (top) and derived result of FFT-analysis with detected whirl modes (bottom). Case: effect of eccentricity and gravity.

From the impact test frequency spectrums it was observed that the lowest Eigen frequency can be found at 18 Hz. This frequency is far away from the excitation frequencies (0.78 Hz and 1.56 Hz) so the system will never excite and never observe resonance.

4. CONCLUSION

Multi-energy domain modelling and simulation was successfully reached using bond graph methodology. CFD simulation of a mixer with a high quality hex mesh was performed and thrust & torque was calculated. It is seen that maximum thrust is generated at zero inlet velocity. Two-way FSI was setup using CFX and APDL code to calculate fluid forces, damping coefficient of water and the final deformation of the blade. Fluid forces and moments were mapped to mass node in a bond graph model of the blade to perform uni-directional fluid-structure interaction including rotor dynamics. The damping coefficient of water was added to system during BG simulation. The blade is vibrating and reaching to final deformation state in less than one second. An impact test was performed and system modal frequencies are calculated. Maximum orbital amplitude and Eigen frequencies of all mechanical components, bearing forces and losses & efficiency of induction motor were calculated, which helps the design engineer for optimization purposes. The model is generic and it could be used for other systems, too. Bond graph is an efficient methodology to model and link together multi-physic dynamic systems and its modularity characteristic permits system growth.

RANS based CFD needs high computational time for one fix boundary condition. The strong coupling of CFD and BG including fluid-induced forces due to the dynamics of involved system components like motor, gearbox and hub is kept as future work for research.

REFERENCES

[1] Wang, X. and Gao, W.D., 1997. “The application of submersible agitator in sewage treatment, Water & Wastewater Engineering”, Vol. 23, pp. 55-56.

[2] Tian, F., Shi, W., Zhang, Q., Zhang, D., & Zhang, G., 2013. Inner flow characteristics at impeller of submersible mixer with two blades. *Journal of Jiangsu University (NSE)*, (34), 395–398.

[3] Kumar, J., Wurm, H. and Sura, H.,2012. “Effect of mixer blade geometry and deformation on jet flow shape and sedimentation in sewage application”. *International Rotating Equipment Conference*, pp. 518–527.

[4] Paynter, H. M., 1961, *Analysis and Design of Engineering Systems*, M. I. T. Press, Cambridge, Mass.,

[5] Karnopp, D.C, Margolis, D.L and Rosenberg, R.C., 1975. *System Dynamics: A Unified Approach.* John Wiley & Sons Inc, pp.414.

[6] Blundell, A.J., 1982. *Bond Graphs for Modelling Engineering Systems.* Ellis Horwood Publishers, pp.151.

[7] Gawthrop,J.,1995. *Physical Model-based Control: A Bond Graph Approach*. *J. Franklin Inst.*, 332B(3), pp.285–305.

[8] Thoma, J.U., 1990. *Simulation by Bondgraphs-Introduction to Graphical Methods*. New York:Springer-Verlag.

[9] Beaman, J.J. and Breedveld, P.C. ,1988. *Physical Modeling With Eulerian Frames and Bond Graphs . J. Dyn. Syst. Control*, 110(2), pp. 7.

[10] Mukerjee, A. and Karmakar, R., 2000. *Modelling and simulation of engineering systems through bondgraphs*. Alpha Science Int’l Ltd.

[11] Campos J, Crawford M, Lane WB, Longoria R. Rotordynamic Modeling Using Bond Graphs : Modeling the Jeffcott Rotor. *IEEE,2004*:164-170

[12] Sanchez R, Medina A. Wind turbine model simulation: A bond graph approach. *Simulation Model. Pract. Theory,2014;*41:24-45.

[13] Van Esch, B.P.M., Van Hooijdonk, J.J.A., Bulten, N.W.H., “Quantification of hydrodynamic forces due to torsional and axial vibrations,” FEDSM2013-16367, *Proceedings of ASME 2013 Fluids Engineering Division Summer Meeting,* Nevada, USA

[14] Kim, J. and Brayant, M.D.,2000. “Bond graph model of a squirrel cage induction motor with direct physical correspondence”. *ASME J. Dyn. Syst. Meas. Control*, Vol. 122, September, pp. 461–469.

[15] Mukherjee, A., Karmakar, R. and Samantaray, A.K., 1999. “Modelling of basic induction motors and source loading in rotor-motor systems with regenerative force field,” Vol. 7, pp. 563–576.

[16] Ghosh, G.C. and Bhadra, S.N., 1993. “Bond Graph Simulation of a Current Source Inverter Driven Induction Motor (Csi–Im) System”. *Electr. Mach. Power Syst.*, 21(1),pp. 51–67.

[17] Hamrock, B.J. and Anderson,W.J., 1983. “Rolling-Element Bearings,” Ohio.

[18] Tolle, G.C.and Muster,D., 1975. *Effect of a Biphase Lubricant on Half Frequency Whirl in a Full Journal Bearing J. Ma*